**Proceedings of CHT-08**
**ICHMT International Symposium on Advances in Computational Heat Transfer**

**May 11-16, 2008, Marrakech, Morrocco**

**CHT-08-P203**

# A SKEW UPWINDING SCHEME FOR NUMERICAL RADIATIVE TRANSFER.

Daniel R. Rousse[⌘,§], Stéphane Lassue[♦]
[⌘]Department of applied sciences, Université du Québec à Chicoutimi, Canada
[♦]LAMTI, Université d'Artois, France
[§]Correspondence author. Fax: +1 418 657 2132. Email: Daniel.Rousse@uquebec.ca

**ABSTRACT** This paper exhaustively presents a skewed upwinding procedure for application to finite volume methods (FVMs), finite element methods (FEMs) or control volume finite element methods (CVFEMs) in the context of radiative heat transfer problems involving participating media. The proposed scheme is based on the application of sound physical arguments. Through its basis of development, this scheme: (1) yields fast convergence of the algorithm; (2) inherently precludes the possibility of computing negative coefficients to the discretized algebraic equations; (3) reduces false scattering (diffusion); (4) is relatively insensitive to grid orientation; and (5) produces solutions completely free from undesirable oscillations. Theses attributes renders the scheme attractive, especially in the context of combined modes of heat transfer and fluid flow problems for which CPU time is a major concern. The suggested first-order skew upwind (SU) scheme has been validated by application to several basic two-dimensional test problems, acknowledged by the radiative heat transfer community: its performance has proven to be excellent. However, the validation is discussed for a few problems only to avoid making this contribution overly lengthy.

## NOMENCLATURE

| | |
|---|---|
| $f^+, f^-, w$ | Weighting functions |
| $G_n^m$ | Geometric quantity, [sr] |
| $\vec{J}_\phi$ | Flux of $\phi$ (radiative) per unit solid angle, [W·m$^{-2}$·sr$^{-1}$] |
| $M$ | Midpoints of element edges |
| $N$ | Number of panels defining a control volume, Node of an element |
| $\vec{n}$ | Unit vector normal to a surface |
| $O$ | Centroid of an element |
| $p$ | Control volume surface (panel) |
| $S_\phi$ | Rate of volumetric generation of $\phi$ |
| $S_I$ | Source of radiative intensity |

**Greek symbols**

| | |
|---|---|
| $\phi$ | Dependent variable |

**Subscripts**

| | |
|---|---|
| $b$ | Blackbody |
| $B$ | Boundary |
| $l$ | Element edge |
| $n$ | Control volume surface (panel) |
| $P$ | Node of reference |
| $r$ | Radiation or Reference point |

| | |
|---|---|
| $\vartheta$ | Integer function: $\vartheta(n) = n$, $\forall n$ = 1, 2, 3; and $\vartheta(n) = n-3$, $\forall n$ = 4, 5 |

**Superscripts**

| | |
|---|---|
| $\rightarrow$ | Vectorial quantity |
| $'$ | Incoming direction |
| $m$ | Discrete direction |

## 1. INTRODUCTION

One of the key issues of the approximate methods that solve the Radiative Transfer Equation (RTE) is the closure relation or spatial interpolation function for the discrete dependent variable intensity over the elements of the computational mesh [Rousse 2000a]. This is then relevant for discrete ordinates methods (DOMs), finite volume methods (FVMs) and control volume finite element methods (CVFEMs).

A first interpolation scheme was introduced by Carlson and Lathrop [1968] in the context of neutron transport problems: it is the diamond difference scheme. This scheme was the first to be implemented by Hyde and Truelove [1976] and later by Fiveland [1984] in their pioneering radiative heat transfer work. It has since been used extensively. However, as for the central difference scheme used in the context of convection diffusion problems, the diamond scheme can produce negative coefficients (elemental negative intensities) in the discretized algebraic equations that represent the original RTE. This procedure may lead to the potential for generating spatially oscillating, physically unrealistic distributions of the transported entity (intensity). Fix-up procedures have been proposed in attempts to solve this problem. All of them result in schemes that require more CPU time per iteration than their original counterpart.

Chai and co-workers [1994a], after testing several procedures, finally recommend to rely on the upwind scheme (US). In that paper, the upwind scheme (or step scheme), the diamond scheme, the positive scheme proposed by Lathrop [1969], and the positive intensity conditions suggested by Fiveland and Jessee [1995], are discussed in the context of the discrete ordinates method. The paper also discusses the relative merits of variable weight schemes proposed by Jamaluddin and Smith [1988] but indicates that, in general, schemes based on weighting factor less than unity could lead to physically unrealistic solutions. Liu *et al.* [1996] showed that the criterion for an unconditionally stable scheme is that this weighting function should be superior to $2/3$.

One of the alternative recommended by Chai and co-workers [1994a], is to trace the downstream intensities at an integration point $p$ to an upstream reference location $r$ where the intensity can be computed or is known in terms of nodal values. This is the basis of the original CVFEM proposed by Rousse and Baliga [1991] and Rousse [1994, 1996, 1997, 2000a]. Although use of unidirectional upwinding (US) removes the potential for spatial oscillations, such a procedure is burdened with excessive false diffusion (false scattering).

The smearing here is numerically (not physically) analogue to what is referred to as false diffusion in the context of fluid flow and convective heat transfer [Patankar 1980]. In this respect, numerical smearing can be referred to as false scattering, which is a numerical redistribution of energy rather than a physical phenomenon. Hence, the authors acknowledge the need for a scheme that models the skewness of radiative transport with improved accuracy.

In the paper of Jessee and Fiveland [1997], the authors address the issue of spatial discretization in the context of numerical smearing. In that paper, the authors state that the upwind scheme is computationally inexpensive but first order accurate thus leading to poor modeling and numerical scattering, and that the diamond scheme modifications, required by the presence of negative coefficients, are not entirely satisfactory. To overcome these drawbacks, the authors investigated bounded high resolution schemes. They concluded that a bounded exponential or higher order

scheme, with built-in flux limiters in which skewness is accounted for, would be promising. However, it could be mentioned that the non-linearity of the proposed high resolution schemes often necessitate an increase in CPU time requirements. It is reported that these high resolution schemes may be competitive with the standard upwind scheme but for significantly scattering media or reflective boundaries.

Liu *et al.* [1996], came to similar conclusions in their analyses of the conventional difference schemes and the SMART scheme. However, the authors recommend the use of the central difference scheme although this scheme may produce spurious oscillations, because it yielded integral quantities (flux, incident radiant energy) almost as accurate as the SMART scheme.

The avenue taken here is somewhat different; instead of using a high order scheme, a first order skew upwind type scheme is proposed. It will be shown that the proposed scheme could be viewed as a skewed positive coefficient upwind scheme limiting the connectivity to a single finite element.

In the context of convection-diffusion and fluid flow problems, false diffusion can be substantially reduced through the use of a skewed upwind scheme such as that proposed by Raithby [1976]. However, this procedure produces the potential for developing spatial oscillations in the solution through the computation of negative coefficients in the discretized equations. Leonard [1979], proposed a quadratic upstream interpolation scheme that considerably reduces the problem. However, his scheme does not entirely circumvent the calculation of negative coefficients. Hassan *et al.* [1983] proposed a procedure that solves the problem by restricting the range of the upstream weighting factor such that the influence coefficients cannot become negative. In some sense, this procedure based on a mathematical restriction on the upstream weighting factor, is akin to a similar ideas developed for the intensity of radiation calculation with the diamond scheme [Lathrop 1969].

Conventional Galerkin finite element methods for convection-diffusion problems experience similar difficulties [Gresho and Lee, 1979] and although several upwind type schemes have been suggested [Christie *et al.* 1976, Heinrich *et al.* 1977, Huyakorn 1977, Hughes *et al.* 1979], they all more or less suffer from false diffusion.

Clearly, in the context of convective transport, a broad range of numerical procedures were proposed in attempts to reduce false diffusion and/or eliminate the negative coefficients problem. Among these, the skewed positive influence coefficient upwinding procedure proposed by Schneider and Raw [1986], modified by Saabas [1991], and by Rousse [1994], was found to hold the premise of a suitable interpolation function for radiation intensity in the context of problems involving radiative heat transfer in participating media.

The present paper is concerned with the progressive development of an interpolation function for radiative intensity that does account for the directionality of the radiant energy propagation through a skewed approach, while simultaneously precluding the possibility of negative coefficients. The development presented in this paper, considers pure upwinding, which is the effect of intensity attenuation and reinforcement are not considered within an element. In this way, the specific features avoiding negative coefficients are readily appreciated. One of the interesting features of the proposed scheme is that it can be used in the context of combined modes heat transfer and fluid flow problems employing the same procedure for the solution of the algebraic discretized conservation equations. Therefore, although implemented in the context of a CVFEM, the ideas are readily amenable for incorporation in a FVM or a FEM.

## 2. CVFEM FORMULATION

The solution of the radiative transfer equation (RTE) by a CVFEM requires the discretizations of both spatial and angular domains. The angular discretization of the RTE, which is solved along *M* discrete directions, leads to the solution of *M* sets of algebraic discretization equations.

**2.1. Radiative Transfer Equation** For the sake of completeness, the multidimensional propagation of radiation in gray-diffuse enclosures filled with gray participating media is recalled here; it can be described by the following equation:

$$\vec{\nabla}\cdot\left(\vec{\Omega}I(s,\vec{\Omega})\right) = -\beta I(s,\vec{\Omega}) + S_I(s,\vec{\Omega}',\vec{\Omega}) \tag{1}$$

where $S_I$, the source function for radiant intensity, is given by:

$$S_I(s,\vec{\Omega}',\vec{\Omega}) = \kappa I_b(s,\vec{\Omega}) + \frac{\sigma}{4\pi}\int_{4\pi} I(s,\vec{\Omega}')\Phi(\vec{\Omega}',\vec{\Omega})d\omega' \tag{2}$$

and the radiative boundary condition at a point *B* on a gray-diffuse surface is:

$$I_B(\vec{\Omega}) = \varepsilon_B I_{b_B}(T_B) + \frac{(1-\varepsilon_B)}{\pi}\int_{(\vec{\Omega}'\cdot\vec{n}_B)<0} \left|\vec{\Omega}'\cdot\vec{n}_B\right| I_B(\vec{\Omega}')d\omega' \tag{3}$$

In the formulation of CVFEMs, it is convenient to cast the governing differential equations in the following general form [Patankar 1980]:

$$\vec{\nabla}\cdot\vec{J}_\phi = S_\phi \tag{4}$$

where $\phi$ stands for a general variable, $S_\phi$ is a volumetric generation rate or source term, and $\vec{J}_\phi$ is the flux of $\phi$. Eq. (1) may be readily obtained from this general equation by using: $\vec{J}_\phi = \vec{\Omega}I(s,\vec{\Omega})$ and $S_\phi = -\beta I(s,\vec{\Omega}) + S_I(s,\vec{\Omega}',\vec{\Omega})$.

**2.2. Domain Discretization** In CVFEMs, the calculation domain is first spatially divided into elements. In a second step of discretization, each element is divided into sub-control volumes in such a manner that upon assembly of elements, complete control-volumes are formed around each node of the computational mesh. In two-dimensional and three-dimensional formulations, three-nodes triangular and four-nodes tetrahedral elements are used in the first step of discretization, respectively. The discussion here is limited to the two-dimensional context.

With regards to angular discretization, discrete ordinates-type or azimuthal discretizations can be used. Discretization details are provided elsewhere [Rousse 2000a].

One should note that FVMs and FEMs do also need spatial and directional discretizations.

**2.3. CVFEM Approximation** An integral conservation equation corresponding to the RTE is obtained by applying the conservation principle to control volumes, *V*, and solid angles, $\omega_m$, such that :

$$\int_{\omega_m}\int_A \vec{J}_\phi\cdot\vec{n}dAd\omega = \int_{\omega_m}\int_V S_\phi dVd\omega \tag{5}$$

where $A$ is the surface area of the control volume, and $\vec{n}$ is a unit outward-pointing normal to the differential area element $dA$.

In the suggested CVFEM, the radiative properties and the scattering phase function are nodal values and are assumed to prevail over the control volume associated with this point and over a discrete solid angle $\omega_m$, while the source term $S_\phi = -\beta I + S_I$ is linearized [Patankar 1980] and assumed constant over control volumes and solid angles. The radiant heat flux is assumed constant over control volume surfaces and solid angles [Rousse 2000a].

The discretized integral conservation equation, corresponding to Eq. (5), in the direction $\vec{\Omega}_m$ for a control volume associated with node $P$ and having $N$ control volume faces is finally:

$$\sum_n^N I_{p_n}^m G_n^m A_n = -\beta_P I_P^m V_P \omega_m + S_{I_P}^m V_P \omega_m \tag{6}$$

where $I_{p_n}^m$ is the intensity evaluated on $p_n$ along $\vec{\Omega}_m$; $G_n^m$ is a geometrical quantity; $A_n$ is the surface area of a control volume surface $p_n$; $I_P^m$ is the intensity evaluated at node $P$ along $\vec{\Omega}_m$; $S_{I_P}^m$ is the value of the source term evaluated at node $P$ in direction $\vec{\Omega}_m$; $V_P$ is the volume surrounding node $P$; and $\omega_m$ is the solid angle associated with direction $\vec{\Omega}_m$.

The geometric function $G_n^m$ is evaluated such that :

$$G_n^m = \int_{\omega_m} (\vec{\Omega} \cdot \vec{n}_n) d\omega \tag{7}$$

where $\vec{n}_n$ is the unit outward-pointing normal to a panel $p_n$. The rational behind these choices is discussed in [Rousse 2000a].

To complete the CVFEM formulation, a relation between the value of the intensity at control volume surfaces and that of this same quantity at the grid nodes of the finite element mesh is required. This relation is established by the prescription of an appropriate spatial interpolation function for intensities over the elements and this is the subject matter of the next section.

The issues of discretization equations, boundary conditions, and solution procedure are presented elsewhere [Rousse 2000a] and are not repeated here to avoid this paper to become overly lengthy.

## 3. SKEW UPWINDING SCHEME

The nature of the discretized RTE does suggest that it is indeed highly desirable not only to account for intensity at upstream locations when closure is needed, but also to reflect the direction of propagation. Here, attention is limited to those two features without regard to attenuation by absorption and out-scattering or reinforcement by emission and in-scattering in the interpolation functions.

The convention adopted here is that depicted in Fig. 1. Careful study of this figure should help the reader in the following sections of the paper. Discussions are limited to the two-dimensional context for simplicity and clarity, but are very exhaustive to help the reader in implementing these ideas, if need be.

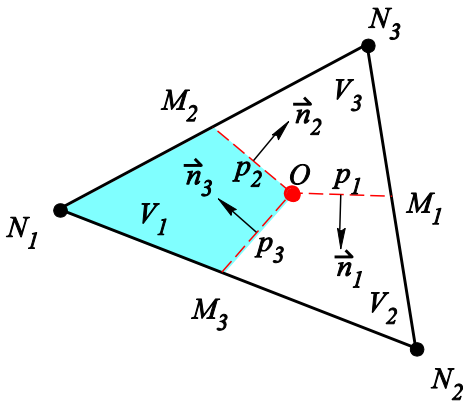


Figure 1 A typical two-dimensional element and its related notation.

**3.1 An Exponential Scheme** The first scheme that was considered for implementation within the CVFEM was the exponential scheme (ES) [Rousse 2000a]. This scheme, based on a particular one dimensional solution of the RTE within an element, yielded very satisfactory predictions [Rousse 1991, 1997, 2000b]. However, this scheme suffers two major drawbacks: (1) it requires fix-up procedures to avoid computations of *negative coefficients*, and (2) exponentials are relatively expensive to compute. Hence, in the context of the development of comprehensive numerical methods for the solution of multiphase turbulent reacting flow combined with radiative heat transfer, such a scheme could lead to unacceptable CPU time requirements.

**3.2 An Upwind Scheme** With the reference to Fig. 2, the implementation of this scheme is rather simple. If the dot product $\vec{\Omega}_m \cdot \vec{n}_{p_1}$ is positive (Fig. 2(a)), the value of the intensity at the integration point $p_1$ is that of the node located immediately counter clockwise with respect to the centroid, *O*, here node $N_3$.

On the other hand, if this dot product is negative (Fig. 2(b)), the value of intensity at the integration point $p_1$ is that of the node located immediately clockwise with respect to the centroid, *O*, here node $N_2$.

For any of the three control volume surfaces (panels), $p_1$, $p_2$, $p_3$, the implementation is straight-forward:

$$I^m_{p_n} = w^m_n I^m_{N_{\vartheta(n+2)}} + (1 - w^m_n) I^m_{N_{\vartheta(n+1)}} \tag{8}$$

where the weighting function $w_n$ is defined as :

$$w^m_n \equiv \mathrm{MAX}\left[\frac{G^m_n}{|G^m_n|}, 0\right] \tag{9}$$

and the integer function $\vartheta(n)$ is such that $\vartheta(n) = n$, $\forall n$ = 1, 2, 3; and $\vartheta(n) = n - 3$, $\forall n$ = 4, 5. The weighting functions, $w^m_n$, for each element, can be evaluated prior to the iterative procedure as they geometric quantities independent of the radiation transfer problem.

The upwind scheme (US) is simple and yields rapid convergence of the solution procedure. Moreover, it ensures that no negative coefficients are produced in the discretization equations.

However, it is obvious that for several discrete directions, the directionality of radiant propagation is not very accurately taken into account. For discrete directions where the node of influence, $N_3$, is in a more or less direct line of sight when observed from the integration point $p_1$, such as in Fig. 2(c), the predictions of intensity along that direction will be good. However, for the situation depicted in Fig. 2(d), *false scattering* (numerical smearing) will occur and for that direction the predictions of radiant intensity will be far less accurate. Moreover, it is clear that this scheme will produce solutions that are very sensitive to the shape of elements. Nevertheless, the upwind scheme (US) was retained as an alternative because it is the simplest scheme and the inaccuracies are averaged over all directions when the radiative fluxes or radiant incident energy are evaluated. Hence, the results for the radiative fluxes and radiant incident energy were found to be in fair agreement with those obtained with higher order schemes.

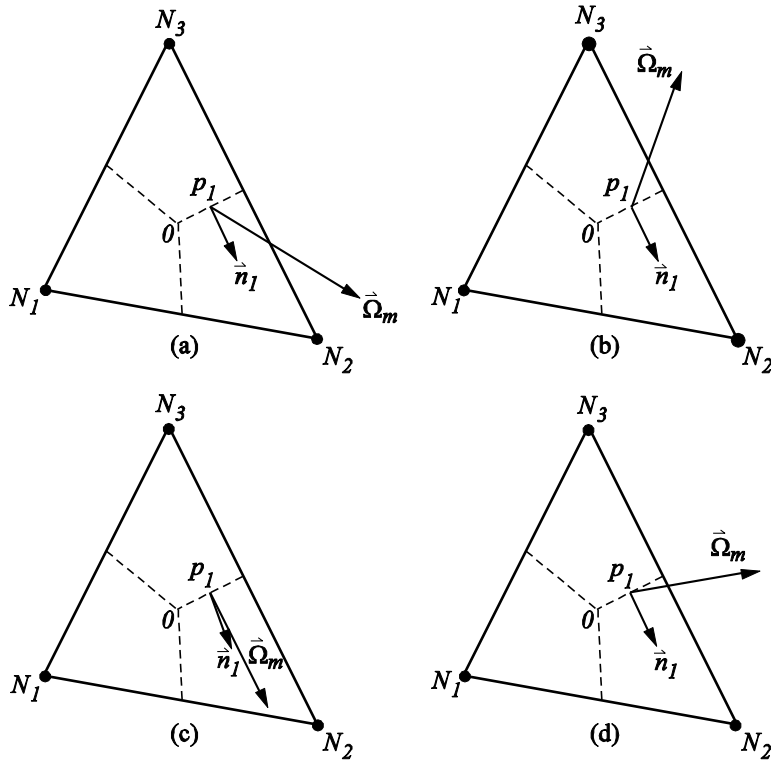


Figure 2: An upwind scheme: (a) Positive dot product; (b) Negative dot product; (c) Fair alignment; and (d) Poor alignment.

**3.3 A Basic Skew Upwind Scheme (BSUS)** With reference to Fig. 3, the basic skew upwind scheme (BSUS), applied to the triangular element discretized into three equal sub-control volumes, determined the value of the intensity at the integration point, $p_1$, by tracking back along the projection of a discrete direction, $\vec{\Omega}_m$, from $p_1$ until the pencil of radiation intersects the element edge at a reference point, *r*. Here, the notation assumes that the edge number, *l*, is that of its corresponding midpoint, *M*. This notation is used for the ease of presentation and implementation.

The value taken for the radiative intensity at *r* is then based on an interpolated value, along this element edge, of the corresponding nodal values (for example, nodes $N_2$ and $N_3$ in Fig. 3(b)). In the context of upwinding, $I^m_{p_n} = I^m_{r_n}$. This leads to a value of the intensity at the integration point that is an average of two nodal values.

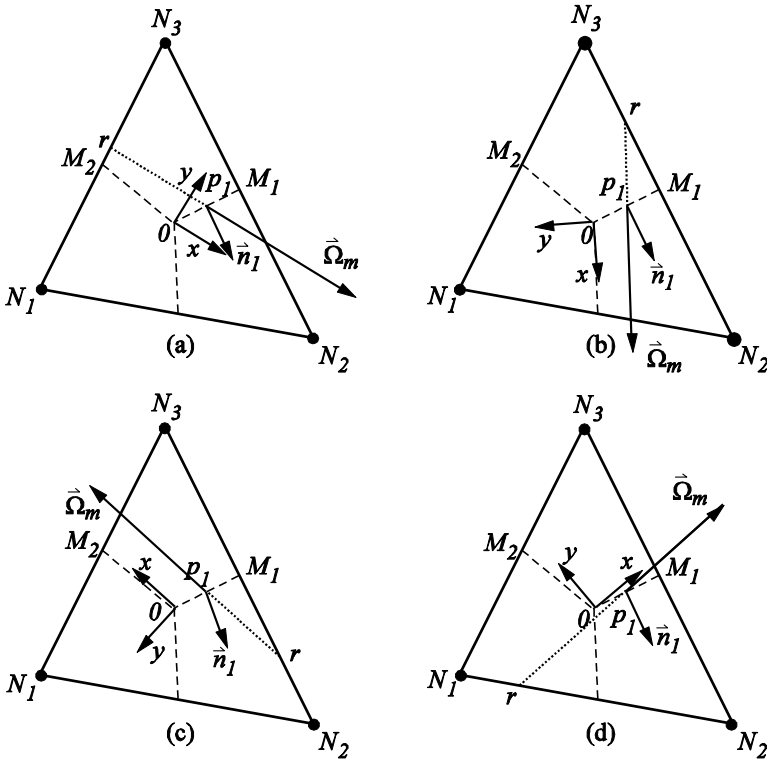


Figure 3: A basic skew upwind scheme: (a) reference node on edge $l$ = 2 linking $N_3$ and $N_1$; (b) reference node on edge $l$ = 1 linking $N_2$ and $N_3$; (c) excellent alignment but reduces to the US; (d) possibility of negative coefficients

When $w_1^m = 1$, see Eq. (9), the reference point will lie either along edge $l = 2$ or $l = 1$. In Fig. 3(a), with respect to a local Cartesian coordinate system located at the centroïd of the element, *O*, that is oriented so as to have its axis *x* aligned with the two dimensional projection of $\vec{\Omega}_m$, the reference point, *r*, lies on the edge $l = 2$ for which: $y_{N_3} \geq y_{p_1} \geq y_{N_1}$. In Fig. 3(b), the reference point, *r*, lies on the edge $l = 1$ for which: $y_{N_2} \geq y_{p_1} \geq y_{N_3}$. In any of these two cases, $I_{p_1}^m$ can be expressed as a linear function of the intensity at two nodes such that:

$$I_{p_1}^m = f_{1l} I_{N_{\vartheta(l+1)}}^m + (1 - f_{1l}) I_{N_{\vartheta(l+2)}}^m \tag{10}$$

where the weighting function $f_{1l}$ in terms of the local and aligned coordinate directions is :

$$f_{1l} = \frac{y_{p_1} - y_{N_{\vartheta(l+2)}}}{y_{N_{\vartheta(l+1)}} - y_{N_{\vartheta(l+2)}}} \tag{11}$$

and *l* is either 1 or 2 according to the relative *y*-coordinate of node $N_3$ with respect to $p_1$.

Similarly, when $w_1^m = 0$, the reference point will lie either along edge $l = 3$ or $l = 1$. In Fig. 3(c), the reference point, *r*, lies on the edge $l = 1$ for which: $y_{N_2} \geq y_{p_1} \geq y_{N_3}$, and the above expression apply. It can readily be observed that the equations are also valid for the case shown in Fig. 3(d) for which: $y_{N_1} \geq y_{p_1} \geq y_{N_2}$. Here, the relative *y*-coordinate of node $N_2$ with respect to $p_1$ determines whether $l = 3$ or $l = 1$.

Generalizing the former expressions, for any of the three control volume surfaces, $p_1$, $p_2$, $p_3$, yields:

$$I_{p_n}^m = f_{nl} I_{N_{\vartheta(l+1)}}^m + (1 - f_{nl}) I_{N_{\vartheta(l+2)}}^m \tag{12}$$

where the expression of $f_{nl}$ is :

$$f_{nl} = \frac{y_{p_n} - y_{N_{\vartheta(l+2)}}}{y_{N_{\vartheta(l+1)}} - y_{N_{\vartheta(l+2)}}} \tag{13}$$

However, this strategy can be challenged for several reasons : (1) for a given direction, when both nodes are located upstream with respect to the integration point $p_1$, such as in Fig. 3(a), there is no guarantee that the intensity at reference point, *r*, will physically be a linear interpolation of the nodal values. Except, may be, in a highly scattering media or when a fine spatial discretization is used; (2) for a particular direction, a node *N* could be located downstream with respect to the integration point such as in Fig. 3(b) where $N_2$ is found to have an influence on $I_{p_1}^m$. This could lead to negative coefficients in the discretized algebraic equations; (3) for some very limited cases only, such as that shown in Fig. 3(c), the scheme would propose a fair representation of the physics (without attenuation). But in this case, it reduces to the US; and (4) for the case represented in Fig. 3(d), the dependence on the intensity at node $N_1$ constitute an *outflow* of radiant energy from the control volume associated with node $N_2$. Thus, if $I_{N_1}^m$ decreases, $I_{N_2}^m$ will increase proportionately. And this clearly shows that *negative coefficients* could be calculated in the numerical solutions.

Remedies to avoid negative coefficients could be thought as follows: (1) when a node *N* is located downstream with respect to the integration point such as in Fig. 3(b), the weighting factor (here $f_{11}$) could be set to zero (when the local *x*-coordinate difference between node $N_2$ and point $p_1$ is positive). Similarly, $f_{11} = 1$ when node $N_3$ is located downstream of point $p_1$; (2) to avoid the outflow problem illustrated in Fig. 3(d), the simplest remedy would be to have an influence of $N_2$ only. Clearly, this overrides the properties of the basic skew upwind scheme (BSUS) and reduces it more or less to the upwind scheme (US).

Nevertheless, having in mind its limitations, the second scheme retained for comparison is the basic skew upwind scheme (BSUS) described by Eq. (12).

**3.4 An Intermediate Skew Upwind Scheme (ISUS)** To avoid having downstream influences and negative coefficients, an intermediate skew upwinding scheme (ISUS) is now introduced. In this scheme, that embeds ideas discussed in the previous subsection, the value of the intensity along the elements edges that link the nodes is assumed to be constant up to the midpoint of the edges: the value of intensity on the edges that delimit sub-control $V_n$ is $I_{N_n}^m$.

With reference to Fig. 4(a), it is seen that line $M_2 - a$ represents a line of discontinuity of the intensity originating from the volumes associated with $N_1$ and $N_3$. The relative influence of both nodes on the value of the radiative intensity at $p_1$ is then a weighted average of $I_{N_3}^m$ and $I_{N_1}^m$, the weights being the ratio $|M_2 - b|/|c - b|$ and $|M_2 - c|/|c - b|$, respectively. On panel $p_1$, $I_{N_1}^m$ prevails from the centroid, *O*, to point *a*, then $I_{N_3}^m$ prevails from *a* to $M_1$. Segment $|c - b|$ is the projection, normal to $\vec{\Omega}_m$, of the control volume surface $p_1$ over edge *l* = 2.

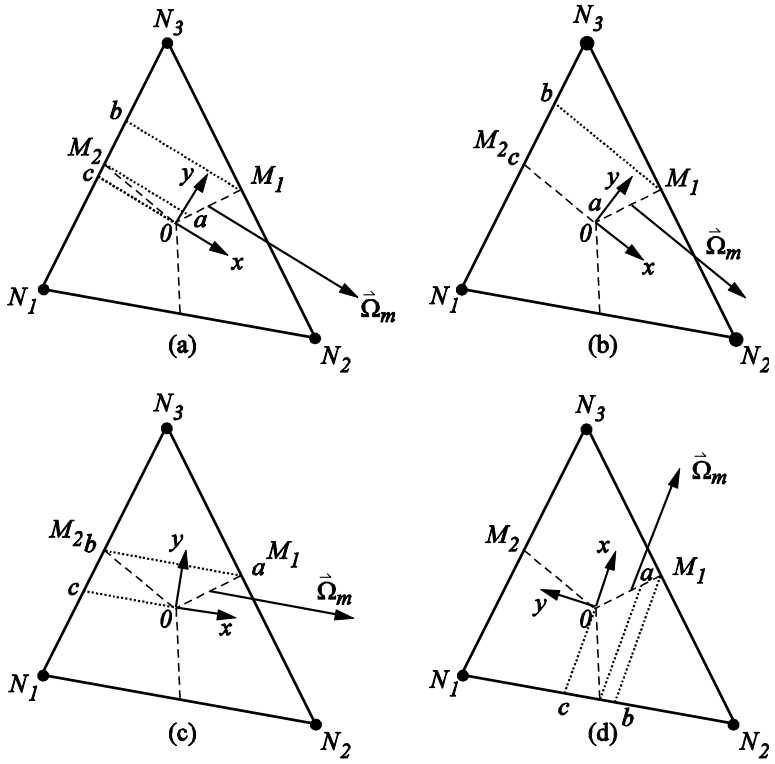


Figure 4: An intermediate skew upwind scheme: (a) weighted average of the intensity at nodes $N_3$ and $N_1$; (b) influence of $N_1$ only when $y_{M_1} \le y_{M_2}$; (c) influence of $N_3$ only when $y_{M_2} \le 0$; and (d) possibility of negative coefficients

When $w_1^m = 1$ (see Eq. (9)), with respect to coordinate axes located at the centroid, *O*, and oriented such that the *x*-axis is aligned with the two-dimensional projection of $\vec{\Omega}_m$, $y_{M_1}$ is positive and as long as $y_{M_2} \le 0$ the node of influence for $p_1$ will be $N_3$ only. The case for which $y_{M_2} = 0$ is shown in Fig. 4(b). When the situation depicted in Fig. 4(a) prevails,

$$I_{p_1}^m = f_1^+ I_{N_1}^m + (1 - f_1^+) I_{N_3}^m \tag{14}$$

where $f_1^+ = y_{M_2} / y_{M_1}$. When $y_{M_2} \ge y_{M_1}$, the node of influence for $p_1$ will be $N_1$ only. Fig. 4(c) depicts the situation for which $y_{M_2} = y_{M_1}$.

To account for the above-described three possibilities, Eq. (14) will be valid if the weighting function is defined such that

$$f_1^+ \equiv \mathrm{MIN}\left[ \mathrm{MAX}\left( \frac{y_{M_2}}{y_{M_1}}, 0 \right), 1 \right] \tag{15}$$

When $w_1^m = 0$, as long as $y_{M_3} \ge 0$ the node of influence for $p_1$ will be $N_2$ only. When the situation depicted in Fig. 4(d) occurs,

$$I_{p_1}^m = f_1^- I_{N_1}^m + (1 - f_1^-) I_{N_2}^m \tag{16}$$

where $f_1^- = y_{M_3} / y_{M_1}$. When $y_{M_3} \le y_{M_1}$, the node of influence for $p_1$ will be $N_1$ only. Hence, with the following weighting function

$$f_1^- \equiv \mathrm{MIN}\left[\mathrm{MAX}\left(\frac{y_{M_3}}{y_{M_1}}, 0\right), 1\right] \tag{17}$$

Eq. (16) provides the value of $I_{p_1}^m$ for the three geometric possibilities with $w_1 = 0$.

Although the expressions for *f* are mathematical expressions evaluated through the determination of the local *y*-coordinate of the element edges midpoints, the resulting expressions have a direct physical interpretation. For example, with respect to the element depicted in Fig. 4(a), it can be seen that $f_1^+$ is the ratio of the radiative flux that crosses control surface $O - M_2$ into direction $\vec{\Omega}_m$ over the radiative flux that crosses control surface $O - M_1$ along the same direction when there is no attenuation or reinforcement within the element. Specifically,

$$f_1^+ \equiv \frac{y_{M_2}}{y_{M_1}} = \frac{\vec{q}_{O-M_2}}{\vec{q}_{O-M_1}} \tag{18}$$

From this expression it can be concluded that the weighting factor will be equal to this ratio as long as the medium in the element, for the purpose of interpolation only, is assumed to be transparent.

Considering $w_1^m$ as defined in Eq. (9), it is possible to account for the negative or positive value of $\vec{\Omega}_m \cdot \vec{n}_{p_1}$ by expressing $I_{p_1}^m$ as

$$I_{p_1}^m = w_1^m [f_1^+ I_{N_1}^m + (1 - f_1^+) I_{N_3}^m] + (1 - w_1^m)[f_1^- I_{N_1}^m + (1 - f_1^-) I_{N_2}^m] \tag{19}$$

Finally, with the use of the integer function $\vartheta(n)$ defined previously, a general mathematical expression of $I_{p_n}^m$ at any of the three panels, $p_1$, $p_2$, $p_3$, can be arrived at :

$$I_{p_n}^m = w_n^m [f_n^{m+} I_{N_m}^m + (1 - f_n^{m+}) I_{N_{\vartheta(n+2)}}^m] + (1 - w_n^m)[f_n^{m-} I_{N_n}^m + (1 - f_n^{m-}) I_{N_{\vartheta(n+1)}}^m] \tag{20}$$

where

$$\begin{aligned} f_n^{m+} &\equiv \mathrm{MIN}\left[\mathrm{MAX}\left(\frac{y_{M_{\vartheta(n+2)}}}{y_{M_n}}, 0\right), 1\right] \\ f_n^{m-} &\equiv \mathrm{MIN}\left[\mathrm{MAX}\left(\frac{y_{M_{\vartheta(n+1)}}}{y_{M_n}}, 0\right), 1\right] \end{aligned} \tag{21}$$

with *n* = 1, 2, 3 for panels $p_1, p_2, p_3$, respectively. The superscript *m* is added to the definition of the weighting function *f* to permit calculation of these functions prior to the iterative solution process.

In Fig. 4(a), the contribution of $N_1$ is still seen by the equations for panel $p_1$ (between the centroid *O* and point *a*), but this contribution has no effect on the radiant energy conservation balance for the control volume associated with $N_3$ after the contribution of $p_2$ is accounted for. Because without

attenuation $I_{p_2}^m$ is $I_{N_1}^m$, all influence of $N_1$ on $p_1$, for this case, cancel. This is valid as long as there is *no attenuation* involved, at the interpolation level, along the propagation path within an element. Otherwise, a net efflux of radiant energy is still possible. That is, if the flux entering $p_2$ is different from that entering $p_1$, between *O* and *a*, *negative coefficients* would still be possible.

The value of the intensity at $p_1$ in Fig. 4(a) is simply a weighted average of that at node $N_1$ and $N_3$. On panel $p_1$, $I_{N_1}^m$ prevails from the centroid to point *a*, then, from *a* to $M_1$, $I_{N_3}^m$ prevails.

**3.5 A Skew Upwind Scheme (SUS) for Numerical Radiative Transfer** The ideas embedded in the skew positive coefficient upwind scheme (SPCUS), which involve a flux-weighted average of the intensity over control volume faces, are first outlined for control volume surface $p_1$ depicted in Fig. 5(a).

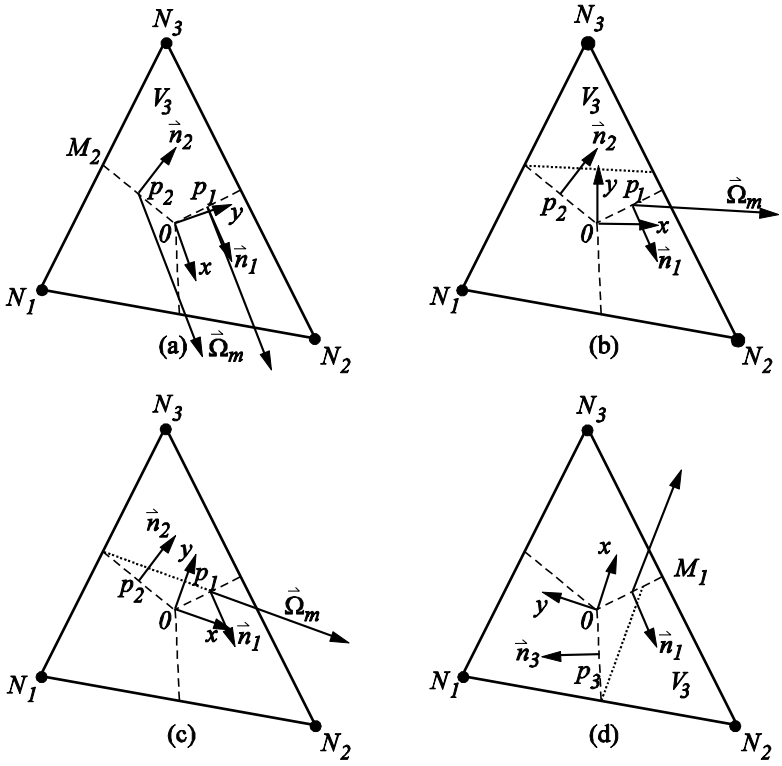


Figure 5: A skew upwinding scheme: (a) influence of $N_3$ only when $y_{M_2} \le 0$; (b) influence of $p_2$ when $y_{M_1} \le y_{M_2}$; (c) weighted average of the intensity at nodes $N_3$ and panel $p_2$; and (d) weighted average of the intensity at nodes $N_2$ and panels $p_3$ when $G_1^m$ is negative

It has been seen that as long as there is *no attenuation* within the elements, the ISUS should improve accuracy over the US and avoid negative coefficients in the discretized algebraic equations. However, in a further refinement of the proposed scheme, it could be desirable to account for attenuation within the element. In this section, for a positive value of the radiant heat flux at $p_1$ (see Fig. 5(a)), that is when $w_1^m = 1$, it is then mostly desirable to express the value of intensity at $p_1$ directly in terms of that at $p_2$ and that at node $N_3$ such that

$$I_{p_1}^m = f_1^{m+} I_{p_2}^m + (1 - f_1^{m+}) I_{N_3}^m \qquad (22)$$

with $f_1^{m+}$ being defined appropriately.

This modification of the ISUS involves that: (1) *negative coefficients can not be computed*, since throughputs of radiant energy are correctly accommodated irrespective of the function $f_1^{m+}$, and (2) a simultaneous set of equations involving the three integration point intensities must be solved to determine these values in terms of the nodal values. To generalize this SPCUS, a similar definition of $f_1^{m+}$ to that used in Eq. (21) is used with the obvious restriction that $0 \leq f \leq 1$.

To ensure a positive contribution to the coefficients when the radiative flux at $p_2$ is *negative* – coming out of sub-control volume $V_3$ in Fig. 5(a) – we need that $I_{p_1}^m = I_{N_3}^m$ : the values of $I_{p_1}^m$ and $I_{p_2}^m$ at the panels $p_1$ and $p_2$ for this situation should only depend on the value of $I^m$ at node 3, which is located upstream of these two surfaces: this implies that $f_1^{m+} = 0$ in Eq. (22). On the other hand, if $G_2^m$ is *positive* – coming into sub-control volume 3 in Fig. 5(b) – and greater than $G_1^m$, only $I_{p_2}^m$ should influence the value of $I_{p_1}^m$, because the amount of energy transported by radiation out of control volume $V_3$ across panel $p_1$ has to be greater than or equal to what comes in by radiation through panel $p_2$, in order to ensure the positiveness of coefficients [Hassan 1983, Rousse 2000a, Saabas 1991]. For this case $f_1^{m+}$ = 1. In other situations, such as in Fig. 5(c), the function $f_1^{m+}$ is just the ratio of the directional integral of $\vec{\Omega} \cdot \vec{n}_p$ over $\omega_m$ for control surface $p_2$ to that over $p_1$. Consequently, a general expression for $f_1^{m+}$, for a *positive* $G_1^m$ can be defined as

$$f_1^{m+} \equiv \mathrm{MIN}\left[ \mathrm{MAX}\left( \frac{G_2^m}{G_1^m}, 0 \right), 1 \right] \tag{23}$$

The subscript 1 stipulates the association with panel 1 and the superscript + indicates that $G_1^m$ is positive.

If these same guide lines are followed when radiation is crossing control volume surface $p_1$ in the negative direction such as in Fig. 5(d) – $G_1^m$ is *negative* – then an equation, involving node 2 and panel $p_3$, can readily be obtained such that

$$I_{p_1}^m = f_1^{m-} I_{p_3}^m + (1 - f_1^{m-}) I_{N_2}^m \tag{24}$$

where $f_1^{m-}$ is defined as

$$f_1^{m-} \equiv \mathrm{MIN}\left[ \mathrm{MAX}\left( \frac{G_3^m}{G_1^m}, 0 \right), 1 \right] \tag{25}$$

Introducing the weighting function, $w_1^m$, defined as in Eq. (9), it is possible to account for the negative or positive value of the radiative flux at $p_1$ by expressing $I_{p_1}^m$ as

$$I_{p_1}^m = w_1^m [ f_1^{m+} I_{p_2}^m + (1 - f_1^{m+}) I_{N_3}^m ] + (1 - w_1^m) [ f_1^{m-} I_{p_3}^m + (1 - f_1^{m-}) I_{N_2}^m ] \tag{26}$$

Finally, with the use of the integer function $\vartheta(n)$ defined previously, a general mathematical expression of $I_{p_n}^m$ at any of the three panels, $p_1, p_2, p_3$, can be arrived at:

$$I_{p_n}^m = w_n^m [ f_n^{m+} I_{p_{\vartheta(n+1)}}^m + (1 - f_n^{m+}) I_{N_{\vartheta(n+2)}}^m ] + (1 - w_n^m)[ f_n^{m-} I_{p_{\vartheta(n+2)}}^m + (1 - f_n^{m-}) I_{N_{\vartheta(n+1)}}^m ] \tag{27}$$

where

$$\begin{aligned} f_n^{m+} &\equiv \mathrm{MIN}\left[ \mathrm{MAX}\left( \frac{G_{\vartheta(n+1)}^m}{G_n^m}, 0 \right), 1 \right] \\ f_n^{m-} &\equiv \mathrm{MIN}\left[ \mathrm{MAX}\left( \frac{G_{\vartheta(n+2)}^m}{G_n^m}, 0 \right), 1 \right] \end{aligned} \tag{28}$$

with $n$ = 1, 2, 3 for panels $p_1, p_2, p_3$, respectively.

## 4. VALIDATION OF THE PROPOSED SCHEME

The following acknowledged standard problems were considered to asses the proposed skew positive coefficient upwinding scheme: (1) gray absorbing media in a rectangular enclosure; (2) gray scattering media in a rectangular enclosure; (3) gray absorbing media in a trapezoidal enclosure; (4) gray absorbing, emitting media in a L-shaped enclosure; and (5) gray absorbing media in a curved Enclosure. However, results are presented for the first, fourth, and fifth problem only to avoid making this paper overly lengthy.

For each demonstration problem, steady-state conditions, homogeneous, constant thermophysical and radiative properties, and radiatively participating gray media are considered [Rousse 2000a]. No relaxation was used in the computations. The iterations were terminated when the absolute value of the residual on the incident radiation *G*, from one iteration to the next, met a prescribed condition $\tilde{\varepsilon}$. In the test problems considered here $\tilde{\varepsilon}$ = $10^{-6}$ was found to be satisfactory : it yielded solutions that were essentially insensitive to further reductions in $\tilde{\varepsilon}$.

Structured-grids, with nodes arranged along straight or curved lines, were employed for all investigations presented here. Various ways of forming triangular elements from quadrilaterals were investigated. The angular discretization was always customized so as to match the physical boundaries of the domain with $\phi - \theta$ azimuthal discretization, except in regular geometries for which standard equal weight $S_n$ discretization were used. Practically, a very fine angular discretization (*ndd* directions) is employed to compute the flux in order to minimize the error due to the quadrature approximation. The refinement is stopped when further increases in the number of directions does not yield a significant change in the solution.

All relevant details are provided herein to allow the reader to implement the problems in his strategy to validate his own numerical method.

For purely absorbing media the *exact* (reference) solution is calculated with:

$$I_P = I_r e^{-\tau} + I_b (1 - e^{-\tau}) \tag{29}$$

where $I_r$ is the intensity at an upstream location along a discrete direction $\vec{\Omega}$, $\tau$ is the optical depth between *r* and *P* measured along $\vec{\Omega}$, and $I_b$ is the blackbody intensity of the media.

**4.1 Gray Absorbing Media in a Rectangular Enclosure**

*4.1.1 Problem statement* In this test case, the proposed CVFEM is applied to a square enclosure filled with an absorbing medium ($\gamma = 0$) at constant temperature $T_m$ = 1. In a first problem, all walls are assumed to be cold, $T$ = 0, except for the third wall in Fig. 6, for which $T_3 = 1$. The absorption coefficient is $\kappa = 0.1\text{m}^{-1}$. In a second problem, $T_3$ is also set to zero. And several optical thicknesses are considered. Here, the dimensionless radiant heat flux, $Q_r$, is set equal to $q_r / (\tilde{\sigma} T_m^4)$.

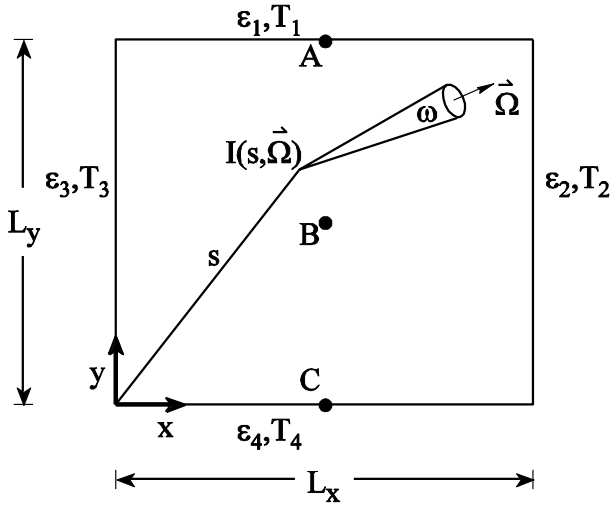


Figure 6: Heat transfer in a rectangular enclosure: problem schematic

*4.1.2 Numerical details and results* The results presented in Fig. 7 show the radiative intensity fields within the domain for the specific direction ($\mu$ = 0.797245675, $\eta$ = 0.577350269). The profiles provided by the US, ES, BSUS, and SUS are compared to the exact solution. The test case has been treated by use of a coarse $21 \times 21$ regular grid, and with an equal weight $S_8$ quadrature. As the medium is at the same temperature than the wall, radiation leaving this wall is maintained at the same level as it travels throughout the domain.

A discontinuity is shown at (0,0) as there is a physical discontinuity imposed between wall 3 and wall 4. Fig. 7(b) and 7(c) indicates that along the discontinuity, the ES and US greatly smear the intensity profile: they introduce false scattering (numerical diffusion). This important numerical diffusion is present as these two schemes are considering only one node of influence at the interpolation level. Consequently, the contributions calculated at control volume faces (panels) do not sufficiently take into account the directionality of the propagation. The BSUS for which the results are presented in Fig.7(d) is very good to reproduce the intensity gradient but spurious numerical oscillations are generated and the results are not physically plausible. This is caused by the influence of downstream nodes on the integrated radiant fluxes at control volume faces for specific directions of propagation. And, as mentioned in the previous section, this produces negative coefficients in the discretization equations. Results for the ISUS are not presented as they are very close to those produced with the SUS. Finally, the SUS shows is capacity to simulating the discontinuity about point (0,0). It reduces numerical diffusion significantly (although the difference in the curve slopes between Fig.7(c) and Fig.7(e) are not that obvious in the figure). This false diffusion is not completely eliminated: the skew upwind scheme is first order. However, it is better that standard upwinding to account for directionality.

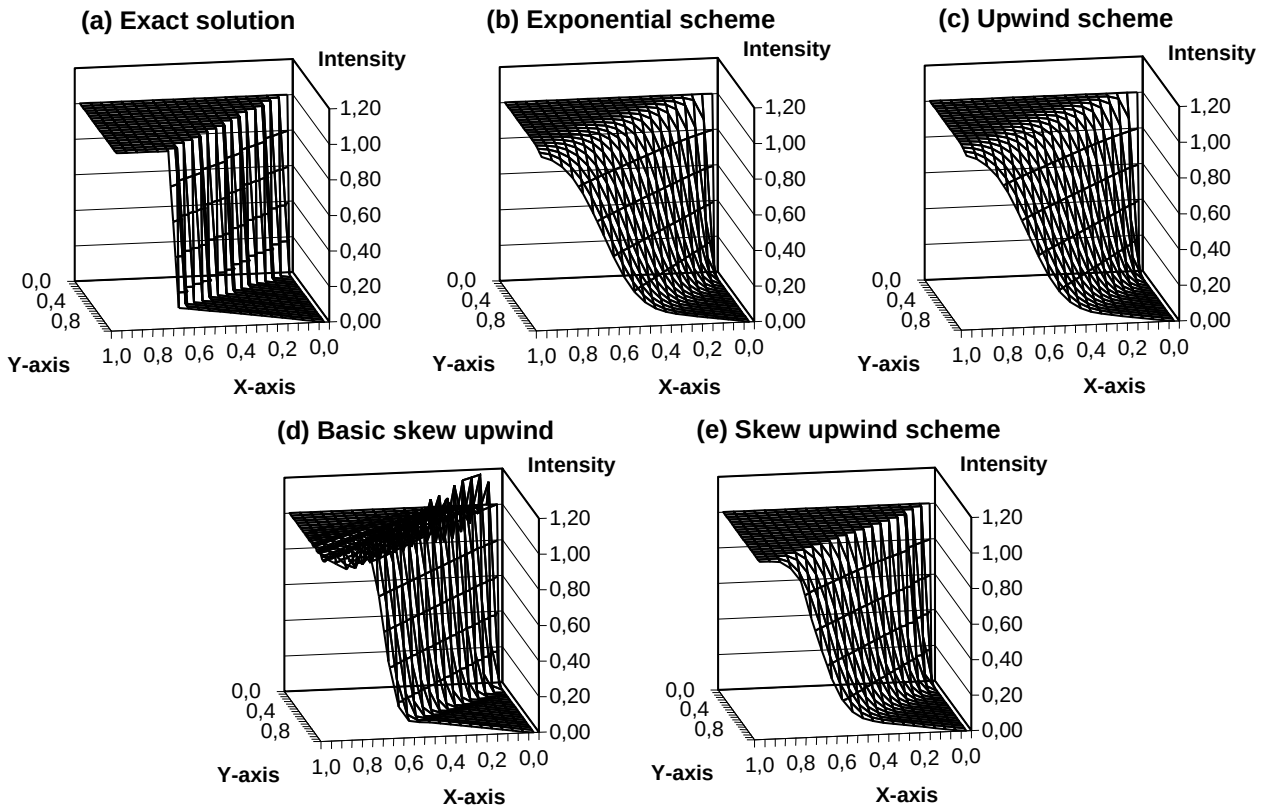


Figure 7: Spatial distribution of intensity for discrete direction ( $\mu$ = 0.797245675, $\eta$ = 0.577350269) in a purely absorbing medium ($T_3$ = 1.0, and $\kappa$ = 0.1 $m^{-1}$) : (a) exact solution; (b) Upwind scheme; (c) Exponential scheme; (d) Basic skew upwind scheme; (e) Skew positive coefficient scheme

In the remainder of the paper, the BSUS will not be considered as the aim is to propose a stable, non oscillating scheme. Moreover, the specifications of commercial CFD codes exclude such types of schemes.

### 4.2 Gray Media in an L-Shaped Enclosure

*4.2.1 Problem statement* This test case involves the irregular-shaped enclosure shown in Fig. 8. The enclosure is assumed to be filled with an emitting, absorbing, and isotropically scattering medium at constant temperature $T_m$, and the walls are assumed to be black and held at a constant zero temperature ($T_w$ = 0), except for the top wall where $T = T^*$. This is equivalent to assuming an outgoing radiant heat flux, $Q_{in}$, on the top wall between point A and point E in Fig. 8. Here, the solutions proposed by Chui [1990] using a FVM are used as references. Chai *et al.* [1994b, 1994c, 1997], Raithby and Chui [1990], and Chui and Raithby [1993] also used this test case to assess their methods. $Q_{in}$ = 1 for purposes of comparison with the solutions proposed in Chui [1990].

*4.2.2 Numerical details and results* In a preliminary series of simulation, two situations were investigated: (1) the absorption coefficient, $\kappa$ = 0.01, and the scattering coefficient, $\sigma$ = 1.00, yielding $\gamma = 1/1.01$; and (2) the case of no scattering, $\sigma$ = 0, with $\kappa$ = 0.01. Grid refinements as well as optical thickness effects were investigated. The above-described furnace involves a particularly interesting feature because the non-orthogonal boundaries make a $45^\circ$ angle with the *x* – *y* coordinate system shown in Fig. 8. Therefore, it is easy to employ a *boundary matching* angular discretization with at least 2 solid angles per quadrant of the *x* – *y* plane.

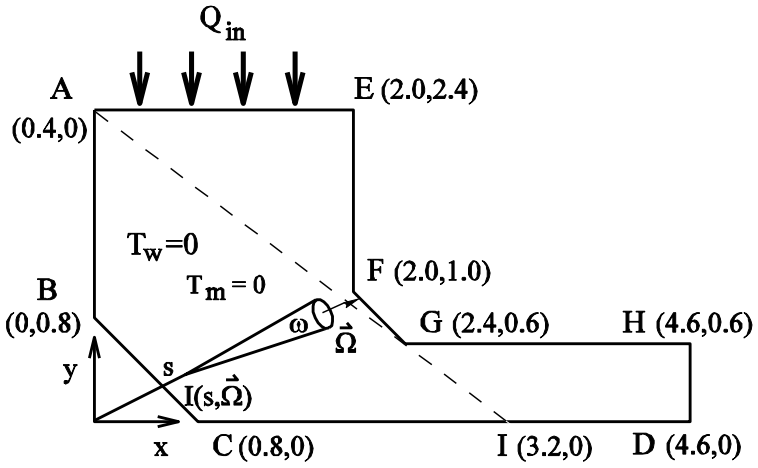


Figure 8: Gray media in an L-shaped two-dimensional enclosure: problem schematic.

Fig. 9 illustrates the dimensionless radiant heat flux, $Q_r$, at the *left-south* wall, identified by points *A*, *B*, *C*, *I*, and *D* in Fig. 13. In Fig. 9(a) the medium both scatters $\sigma$ = 1.00 and absorbs $\kappa$ = 0.01 radiant energy while, in Fig. 9(b), the medium absorbs $\kappa$ = 0.01 radiant energy only. In Chui [1990], the investigator employed a relatively coarse $11\times4$ spatial grid and an angular discretization that involved 2 latitudes and 8 longitudes within an octant. For this test case, the first spatial computational domain employed with the proposed method consisted of 52 irregular quadrilaterals, each divided into two triangular elements, and the angular grid was constructed using 16 discrete directions, that is one latitude in the positive *z* direction and 4 discrete solid angle in each quadrant of the $x-y$ plane. A finer grid involving $33\times15$ nodes and 64 directions distributed on two latitudes was also employed for direct comparison with Rousse [1994]. In the notation involved in the legend of the figures, the discretization is identified with 4 numbers: the first number refers to the number of grid nodes along the left-south wall (*A-B-C-I-D*) and right-north wall (*E-F-G-H*) of the enclosure depicted in Fig. 8; the second number is the number of grid nodes used on the top wall (*A-E*) and right wall (*H-D*); the third number refers to the number of latitudes employed with the azimuthal angular discretization; and the last number is the number of solid-angle projections in each quadrant of the $x-y$ plane.

In Fig. 9(a), the surface radiant heat flux, $Q_r$, along the left-south wall (*A-B-C-I-D*), decreases with the distance away from point *A*, measured between *A* and *D*, because radiation is attenuated by absorption and scattering as it travels away from the top (hot) wall. When there is no scattering, $\gamma = 0$ in Fig. 9(b), the radiant heat flux impinging on a surface is very sensitive to the orientation of this surface with respect to the source $Q_{in}$ (located on the top wall).

In Fig. 9(b) it can be observed that the FVM $11\times4$ fails to predict the two bumps, that correspond to locations *B* and *C*, in the surface radiant heat flux distribution. Chui's solution [1990] indicates a plateau while the $13\times4$ CVFEM solution shows the two peaks at point *B* and *C*. The CVFEM solution for a coarse grid is shown somewhat better than its corresponding FVM counterpart. This may be caused by the treatment of the boundary conditions and by the fact that in the CVFEM each quadrilateral is divided into two triangular elements. This yields a finer discretization and hence a better approximation of the radiative fluxes across control volume surfaces.

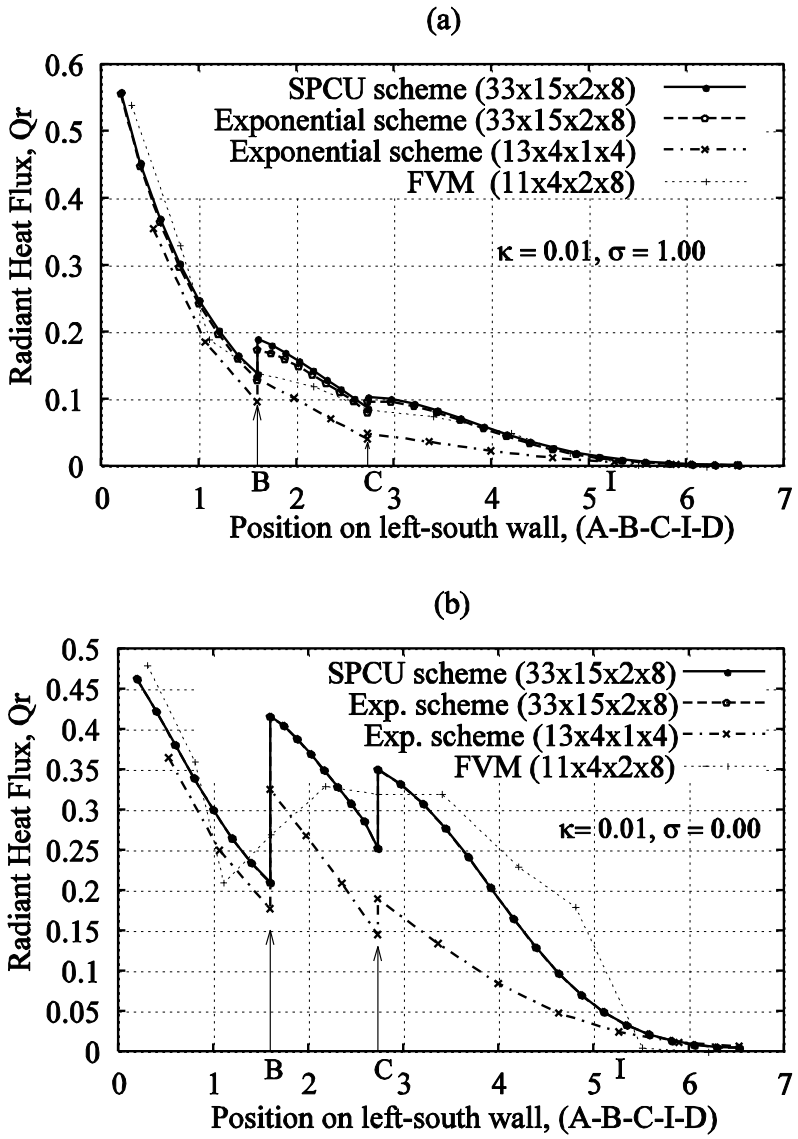


Figure 9: Distribution of dimensionless radiant heat flux, $Q_r$, on the left-south wall *A-B-C-I-D* for : (a) $\kappa$ = 0.01, $\sigma$ = 1.0; (b) $\kappa$ = 0.01, $\sigma$ = 0.0.

The orientation of the wall changes at *B* and *C*, and this makes the left-south wall lie in a more direct line of sight from the source of radiation on the top wall (*A-E*). There should be discontinuities in the $Q_r$ distribution at *B* and *C* for $\sigma = 0$. The tendency is well predicted by the relatively fine grid ($33 \times 15$ nodes) combined with fine angular discretization involving 64 directions (2 latitudes and 8 projections per quadrant). To capture the flux discontinuities, grid points should be inserted close to points *B* and *C*. Beyond point *C*, along *C-D*, after the step *B-C*, the radiant heat flux is seen to decrease to zero as some points (beyond point *I*) do not "see" the radiation source on the top wall *A-E*, and because there is no reflection and no emission from the boundaries. When scattering is present, Fig. 9(a), the changes in the distribution of the radiant heat flux at point *B* and *C* are less pronounced because a direct line of sight to *A-E* is less important than in the case of no scattering in Fig. 9(b). Chui's solution [1990] and the coarse CVFEM solution indicate monotonic decrease of the radiant heat flux along the left-south wall, whereas the CVFEM solution obtained with a fine grid, which reproduces the physics more faithfully, shows the expected bumps at point *B* and *C*.

The radiant heat flux at the *right-north* wall (*E-F-G-H* in Fig. 8) was also computed [Rousse 2000] (but not shown herein) with more accuracy with the CVFEM than with the FVM of Chui [1990]. The effect of angular and spatial discretization refinement and that of optical thickness were also investigated. Interested readers should consult the corresponding author for details.

Figure 9 indicates that results for the ES and SUS more or less correspond for the prediction of the radiative flux and that despite the superiority of the skew upwind scheme over the exponential scheme in predicting the discrete value of the radiative intensity in one particular direction. When integrated values are calculated (such as the heat flux), the errors are more or less averaged over all directions.

### 4.3 Gray Absorbing Media in a Curved Enclosure

*4.3.1 Problem statement* In this last test case, a quarter of circle – with a rectangular region added on its top – was used as a test geometry. In Fig. 10, the curve wall is hot, $T_4 \neq 0$, and black while all other walls are cold, $T_1 = T_2 = T_3 = 0$. The medium is cold and purely absorbing with $\kappa = 1$. The radius of the quarter of circle is equal to the length along the *x*-axis, $L_x = 1.0$, and $L_y = 1.5$. Chai *et al.* [1994c, 1995] and Liu *et al.* [1997] used that problem.

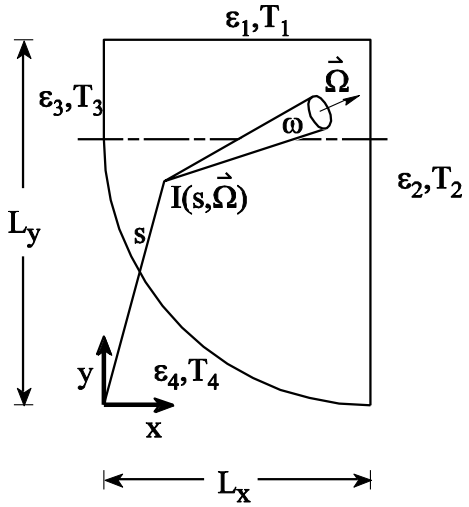


Figure 10: Gray media in a curved computational enclosure: problem schematic

*4.3.2 Numerical details and results* A $37 \times 37$ spatial grid and an azimuthal $20 \times 4$ grid in the $\phi$ and $\theta$ directions were employed with a progressive deployment of the spatial grid: there are more nodes in the immediate vicinity of the walls. This discretization was found to be required to ensure grid independent solutions with further refinements.

The predictions of the radiant heat flux on the right wall (wall 2) are reported in Fig. 11. It is globally shown that the CVFEM solution, using the skew upwind scheme, is in good agreement with that proposed by Chai *et al.* [1995] although detailed (or refined) comparisons was not possible due to the type of results presented in the reference. But the interesting fact here is that the overall solution is slightly scheme dependent with the same discretization. Nevertheless, as for the preceding problem, here also results for the three schemes show that despite the superiority of the SUS scheme over the others in predicting the discrete value of the radiative intensity in one particular direction, the errors are more or less averaged over all directions.

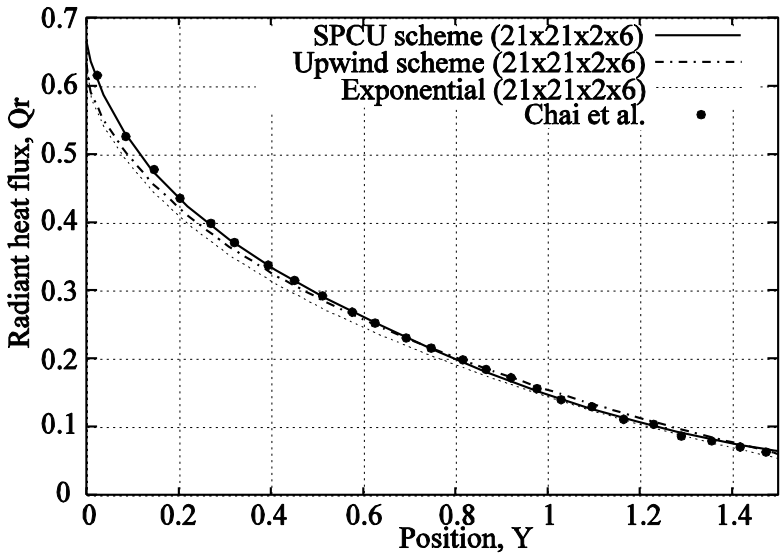


Figure 16: Distribution of dimensionless radiant heat flux, $Q_r$, on the right surface for absorbing media bounded by a black curved enclosure, $\beta$ = 1.

## CONCLUSION

This paper presented the detailed derivation of a skew upwind (SU) scheme for the computation of radiative transport in enclosures filled with participating media. The exhaustive description was intended for the analyst who may want to implement such a procedure in his or her own numerical method. The proposed scheme is based on the application of sound physical arguments, resulting in: (1) fast convergence of the algorithm; (2) inherent preclusion of the possibility of computing negative coefficients to the discretized algebraic equations; (3) relatively low levels of false scattering; (4) relative insensitivity to grid orientation; and (5) solutions completely free from undesirable oscillations. These attributes render the scheme attractive, especially in the context of combined modes of heat transfer and fluid flow for which CPU time is a major concern. The performances of the proposed scheme are readily available in the following paper

However, results show that despite the superiority of the SU scheme over the upwind scheme (US), in predicting the discrete value of the radiative intensity in one particular direction, when integrated values are calculated, the errors are more or less averaged over all directions. Hence, despite an increase of about 20% in CPU time requirement, the difference between the SU scheme and the simple US diminishes substantially.

## APPENDIX A: CLOSURE RELATIONS

Eqs. (8), (12), (20), and (27) are systems of equations for the unknowns $I_p^m$. These systems of equations can conveniently be written in a matrix form, yielding

$$[A]_{3\times3}\{I_p^m\}_{3\times1} = [B]_{3\times3}\{I_N^m\}_{3\times1} \tag{31}$$

or

$$\begin{bmatrix} a_{11} & a_{12} & a_{13} \\ a_{21} & a_{22} & a_{23} \\ a_{31} & a_{32} & a_{33} \end{bmatrix} \begin{Bmatrix} I_{p_1}^m \\ I_{p_2}^m \\ I_{p_3}^m \end{Bmatrix} = \begin{bmatrix} b_{11} & b_{12} & b_{13} \\ b_{21} & b_{22} & b_{23} \\ b_{31} & b_{32} & b_{33} \end{bmatrix} \begin{Bmatrix} I_{N_1}^m \\ I_{N_2}^m \\ I_{N_3}^m \end{Bmatrix} \tag{32}$$

**A.1 Upwind scheme** For a two-dimensional implementation of the upwind scheme (US), the A matrix is the identity matrix while the coefficients of the B matrix are:

$$b_{jj} = 0;\ \ b_{j,\vartheta(j+1)} = (1 - w_j^m);\ \ b_{j,\vartheta(j+2)} = w_j^m \tag{33}$$

Basic skew upwind scheme

To implement the basic skew upwind scheme in two-dimensions, the A matrix is also the identity and matrix B can be constructed such that, when $y_{N_j} \geq y_{p_i} \geq y_{N\vartheta(j+1)}$, we obtain :

$$b_{ij} = f_{ij};\ \ b_{i,\vartheta(j+1)} = (1 - f_{ij});\ \ b_{i,\vartheta(j+2)} = 0 \tag{34}$$

**A. 2 Intermediate skew upwind scheme** To implement the basic skew upwind scheme in two-dimensions, the A matrix is once again the identity matrix and matrix B can be constructed such that:

$$b_{jj} = w_j^m f_j^{m+} + (1 - w_j^m) f_j^{m-};\ \ b_{j,\vartheta(j+1)} = (1 - w_j^m)(1 - f_j^{m-});\ \ b_{j,\vartheta(j+2)} = w_j^m (1 - f_j^{m+}) \tag{35}$$

The full matrix coefficients for the ISU scheme are :

$$\begin{bmatrix} w_1^m f_1^{m+} + (1 - w_1^m) f_1^{m-} & (1 - w_1^m)(1 - f_1^{m-}) & w_1^m (1 - f_1^{m+}) \\ w_2^m (1 - f_2^{m+}) & w_2^m f_2^{m+} + (1 - w_2^m) f_2^{m-} & (1 - w_2^m)(1 - f_2^{m-}) \\ (1 - w_3^m)(1 - f_3^{m-}) & w_3^m (1 - f_3^{m+}) & w_3^m f_3^{m+} + (1 - w_3^m) f_3^{m-} \end{bmatrix}$$

**A.3 Skew positive coefficient upwind scheme** For the implementation of the skew positive coefficient upwind scheme (SPCUS), the coefficients of matrices A and B are

$$\begin{aligned} &a_{jj} = 1;\ \ a_{j,\vartheta(j+1)} = -w_j^m f_j^{m+};\ \ \ \ a_{j,\vartheta(j+2)} = -(1 - w_j^m) f_j^{m-} \\ &b_{jj} = 1;\ \ b_{j,\vartheta(j+1)} = (1 - w_j^m)(1 - f_j^{m-});\ \ b_{j,\vartheta(j+2)} = w_j^m (1 - f_j^{m+}) \end{aligned} \tag{36}$$

The matrix coefficients for the SPCU scheme are :

$$\begin{bmatrix} 1 & -w_1 f_1^+ & -(1 - w_1) f_1^- \\ -(1 - w_2) f_2^- & 1 & -w_2 f_2^+ \\ -w_3 f_3^+ & -(1 - w_3) f_3^- & 1 \end{bmatrix}$$

$$\begin{bmatrix} 0 & (1 - w_1)(1 - f_1^-) & w_1 (1 - f_1^+) \\ w_2 (1 - f_2^+) & 0 & (1 - w_2)(1 - f_2^-) \\ (1 - w_3)(1 - f_3^-) & w_3 (1 - f_3^+) & 0 \end{bmatrix}$$

These matrices involve geometric quantities only. They can be computed before the iterative solution procedure that solves for intensity begins.

**Acknowledgment :** The authors gratefully acknowledge Rodolphe Vaillon (CNRS researcher, CETHIL, INSA de Lyon), Guillaume Gautier (Eng, PSA Group), and Mathieu Francoeur (Researcher, University of Kentucky) for their participation, collaboration and/or comments during these research works. The authors are also grateful to the Natural Sciences and Engineering Research Council of Canada (NSERC). Thanks go to Alan Wright for helping in the preparation of this manuscript.

## REFERENCES

Carlson, B.G., and Lathrop, K.D. [1968], Transport Theory – The method of Discrete-Ordinates, *In Computing Methods in Reactor Physics*, Gordon and Breach, New York.

Chai, J.C., Patankar, S.V., and Lee, H.S. [1994a], Evaluation of Spatial Differencing Practices for the Discrete-Ordinates Method, *J. Thermophys. Heat Transfer*, Vol. 8, no. 1, pp 140-144.

Chai, J.C., Lee, H.S. and Patankar, S.V. [1994b], Improved Treatment of Scattering using the Discrete Ordinates Method, *ASME J. Heat Transfer*, Vol. 116, pp 260-263.

Chai, J.C., Lee, H.S. and Patankar, S.V. [1994c], Treatment of Irregular Geometries using a Cartesian Coordinates Finite-Volume Radiation Heat Transfer Procedure, *Num. Heat Transfer, Part B*, Vol. 26, pp 225-235.

Chai, J.C., Parthasarathy, G., Lee, H.S. and Patankar, S.V. [1995], Finite-Volume Radiative Heat Transfer Procedure for Irregular Geometries, *J. Thermophys. Heat Transfer*, Vol. 9, no.3, pp. 410-415.

Christie, I., Griffiths, D.F. Mitchell, A.R. and Zienkiewicz, O.C. [1976], Finite Element Methods for Second Order Differential Equations with Significant First Derivatives, *Int. J. Numer. Methods Eng*., Vol. 10, pp 1389-1396.

Chui, E.H. [1990], Modelling of Radiative Heat Transfer in Participating Media by the Finite Volume Method, *Ph.D. thesis*, University of Waterloo, Canada.

Chui, E.H. and Raithby, G.D. [1993], Computation of Radiant Heat Transfer on a Non-Orthogonal Mesh using the Finite Volume Method, *Num. Heat Transfer, Part B*, Vol. 23, pp. 269-288.

Fiveland, W.A. [1984], Discrete-Ordinates Solutions of the Radiative Transport Equation for Rectangular Enclosures, *ASME J. Heat Transfer*, Vol. 106, no. 2, pp. 699-706.

Fiveland, W.A., and Jessee, J.P. [1995], Comparisons of Discrete Ordinates Formulations for Radiative Heat Transfer in Multidimensional Geometries, *J. Thermophys. Heat Transfer*, Vol. 9, pp 47-54.

Gresho, P.M. and Lee, R.L. [1979], Don't Suppress the Wiggles – They're Telling you Something!, In Proc. Symposium Finite Element Methods for Convection Dominated Flows, pp. 37-61, *ASME Winter Ann. Meeting*, New York.

Hassan, Y.A. Rice, J.G. and Kim, J.H. [1983], A Stable Mass-Flow-Weighted Two-Dimensional Skew Upwind Scheme, *Num. Heat Transfer*, Vol. 6, pp 395-408.

Heinrich, J.C., Huyakorn, P.S., Zienkiewicz, O.C. and Mitchell, A.R. [1977], An Upwind Finite Element Method Scheme for Two-Dimensional Convective Transport Equations, *Int. J. Numer. Methods Eng*., Vol. 11, pp 131-143.

Hughes, T.J.R., Liu, W.K. and Brooks, A.N. [1979], Finite Element Analysis of Incompressible Viscous Flows by the Penalty Function Formulation, *J. Comp. Phys*., Vol. 30, pp 1-60.

Huyakorn, P.S. [1977], Solution of Steady-State Transp Element Scheme, *Appl. Math, Modelling*, Vol. 1, pp 187-195.

Hyde, D.J. and Truelove, J.S. [1976], The Discrete Ordinates Approximations for Multidimensional Radiant Heat Transfer in Furnaces, *Technical Report, UKAEA*, Report number AERE-R8502.

Jamaluddin A.S., Smith, P.J. [1988], Predicting Radiative Transfer in rectangular Enclosures using the Discrete Ordinates Method, *Combust. Sci. Tech*, Vol. 59, pp 321-340.

Jessee, J.P. and Fiveland, W.A. [1997], Bounded, High-Resolution Differencing Schemes Applied to the Discrete Ordinates Method, *J. Thermophys. Heat Transfer*, Vol. 11, pp. 540-548.

Lathrop, K.D. [1969], Spatial Differencing of the Transport Equation: Positivity vs Accuracy, *J. Comp. Physics*, Vol. 4, pp 475-498.

Leonard, B.P. [1979], A Stable and Accurate Convective Modelling Procedure Based on Quadratic Upstream Interpolation, *Comp. Meth. In App. Mech. and Eng*., Vol. 19, pp 59-98.

Liu, F., Becker, H.A. and Pollard, A. [1996], Spatial Differencing Schemes of the Discrete-Ordinates Method, *Num. Heat Transfer, Part B*, Vol. 30, pp 23-43.

Liu, J., Shang, M. and Chen, Y.S. [1997], Prediction of Radiative Transfer in General Body-Fitted Coordinates, *Num. Heat Transfer, Part B*, Vol. 31, pp 423-439.

Patankar, S.V. [1980], Numerical Heat Transfer and Fluid Flow, *Hemisphere*, Washington.

Raithby, G.D. [1976], Skew Upstream differencing Schemes for Problems Involving Fluid Flow, *Comp. Meth. In App. Mech. and Eng*., Vol. 9, pp 153-164.

Raithby, G.D. and Chui, E.H. [1990], A Finite-Volume Method for Predicting Radiant Heat Transfer in Enclosures with Participating Media, ASME J. Heat Transfer, vol. 112, no. 2, pp. 415-423, 1990.

Rousse, D.R. and Baliga, R.B. [1991], Formulation of a Control-Volumes Finite Element Method for Radiative Transfer in Participating Media, *In* Proc. *7th Int. Conf. Num. Meth. Thermal Problems*, pp 786-795, Stanford.

Rousse, D.R. [1994], Numerical Predictions of Multidimensional Conduction, Convection and Radiation Heat Transfer in Participating Media, *Ph.D. thesis*, McGill University, Montréal.

Rousse, D.R. [1996], Numerical Method for Conduction-Convection-Radiation Heat Transfer in Three-Dimensional Geometries, *In* Proc. *2nd European Thermal Sciences* and *14th UIT conference*, Vol. 3, Rome, pp 1425-1432.

Rousse, D.R. [1997], Le Couplage d'une Méthode pour Prédire le Rayonnement avec les Codes de CFD: Capacités et Limitations d'une CVFEM, *In* Compte-Rendus : *Congrès de la Société Française des Thermiciens*, Toulouse, pp 538-544.

Rousse, D.R. [2000a], Numerical Predictions of Two-Dimensional Conduction, Convection, and Radiation Heat Transfer. I – Formulation, *Int. J. Thermal Sciences*, Vol. 39, no. 3, pp 315-331.

Rousse, D.R., Gautier, G. and Sacadura, J.F. [2000b], Numerical Predictions of Two-Dimensional Conduction, Convection, and Radiation Heat Transfer. II – Validation, *Int. J. Thermal Sciences*, Vol. 39, no. 3, pp 332-353.

Saabas, H.J. [1991], A CVFEM for three-Dimensional, Incompressible, Viscous Fluid Flow, *Ph.D. thesis*, McGill University, Montréal.

Schneider, G.E.. and Raw, M.J. [1986], A Skewed Positive Influence Coefficient Upwinding Procedure for Control Volume Based Finite Element Convection Diffusion Computation, *Num. Heat Transfer*, Vol. 9, pp 1-26.

Talukdar**,** P. [2006], Radiative heat transfer for irregular geometries with the collapsed dimension method, *Int. J. Thermal Sciences*, Vol. 45, no 2, February 2006, pp 103-109.